Proceedings of the Canadian Society for Mechanical Engineering International Congress
32nd Annual Conference of the Computational Fluid Dynamics Society of Canada
Canadian Society of Rheology Symposium
CSME-CFDSC-CSR 2025
May 25–28, 2025, Montréal, Québec, Canada

Vibration Analysis of Robot Manipulators and Gaussian Process Regression for Estimating Posture-dependent FRF

Seyed Hamed Seyed Hosseini1,2, Seyedhossein Hajzargarbashi2, Zhaoheng Liu1*
1Department of Mechanical Engineering, École de technologie supérieure, Université du Québec, 1100 Notre-Dame St W, Montreal, H3C 1K3, Canada
2Aerospace Manufacturing Technologies Centre, National Research Council Canada, 2107 Chemin de Polytechnique, Montreal, Quebec, H3T 1J4, Canada
* Corresponding author: seyed-hamed.seyed-hosseini.1@ens.etsmtl.ca
Contributing authors: Zhaoheng.Liu@etsmtl.ca; Seyedhossein.Hajzargarbashi@cnrc-nrc.gc.ca

Abstract— This study investigates the vibration behavior of robot manipulators using both experiments and numerical analysis. A key challenge is identifying posture-dependent vibration modes and understanding how accelerometer placement affects measurements. Hammer tests are conducted at about 250 robot postures along different tool-tip directions to obtain frequency response functions (FRFs). Results show that lower vibration modes (modes 1–3) are influenced by the first three joints due to their larger masses. However, in a continuous system such as a robot, all vibration modes can be affected by all joints and components. A dataset of joint angles and modal parameters is created and used to train a Gaussian Process Regression (GPR) model, which accurately predicts vibration behavior while reducing computational costs. The study provides a step-by-step method for experimental modal analysis, improves understanding of joint-vibration relationships, and offers a data-driven GPR approach for efficient vibration analysis in robotic machining and industrial applications. Finally, an estimate of the FRFs using the predicted modal parameters is provided while they are compared with the experimental results.

Keywords: Vibration analysis; Modal parameter identification; Gaussian Process Regression (GPR); Frequency response function (FRF); Experimental Modal Analysis (EMA);

I. Introduction

Traditional industrial robots are valued for their cost-effectiveness, large workspaces, and adaptability in machining complex geometries like aircraft components [1, 2]. However, joint-induced vibrations limit their precision, particularly in high-accuracy tasks [3]. These vibrations, often linked to the "chatter" phenomenon during machining, are influenced by dynamic instabilities and posture-dependent flexibility [4, 5]. While tools like Frequency Response Functions (FRFs) capture vibrational behavior, existing studies using Experimental/Operational Modal Analysis (EMA/OMA) and simulations [6-8] only broadly acknowledge posture-dependent dynamics without detailing how specific joints or modes contribute to energy absorption. This oversight limits actionable insights for vibration mitigation, as highlighted by Iglesias et al. [9], who emphasize the need for deeper analysis of stiffness and resonant frequency interactions.

To address this gap, recent advances propose combining experimental data with machine learning. For instance, Nguyen et al. [10, 11] integrated Gaussian Process Regression (GPR) with OMA to predict modal parameters, reducing testing requirements while maintaining accuracy. Building on these approaches, this study introduces a three-phase framework: (1) systematic hammer tests across postures to map FRF variations, (2) data refinement to isolate posture-dependent trends, and (3) a tailored GPR model with adaptive kernels to predict FRFs for unseen configurations. Unlike prior work [12, 13], this method connects how individual joints move to the overall vibration patterns of the entire system, aiming to enhance predictive accuracy while minimizing computational costs. By bridging experimental and analytical insights, the research seeks to advance robotic machining precision and broaden industrial applications.

II. Vibration Analysis of the Robot Manipulators

A. Experimental Test Design and Analysis of Measured Data

This section investigates how vibrations behave in a 6-degree-of-freedom (DOF) KUKA robot by testing it across 254 different postures within its workspace. The goal is to pinpoint which joints and vibration modes most critically affect its performance. To do this, hammer tests and EMA were conducted at specific points along a predefined trajectory

(Figure 1) to ensure the robot's joints were positioned at unique angles for each test. By analyzing these postures, the study aimed to uncover how joint configurations influenced vibrational patterns, such as resonance or damping effects.

The process began by defining 254 points across the robot's workspace, where its end-effector (tool tip) was precisely positioned. At each point, three hammer strikes in the X, Y, and Z directions were applied to the tool tip, and acceleration signals were recorded using a triaxial accelerometer. A Siemens LMS SCADAS system collected data at 1024 Hz with 0.25 Hz resolution, paired with an impact hammer and sensor setup. This systematic approach ensured high-resolution vibration data and enabled detailed analysis of posture-dependent dynamics and joint-specific contributions to vibrational modes.

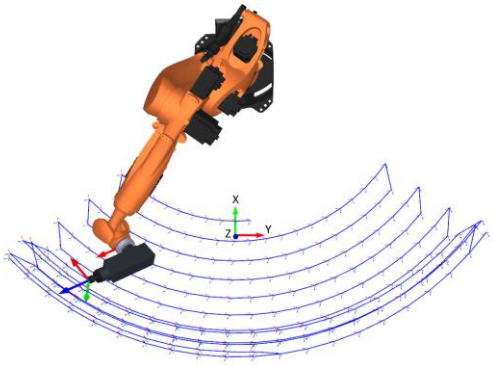

Figure 1: The end-effector trajectory within the restrained workspace with 254 positions.

To ensure accurate identification of natural frequencies, damping ratios, and modal stiffness values from vibration data, a robust four-step post-processing method was developed. First, peaks in the FRFs were visually inspected. Second, phase changes and coherence values were analyzed to filter out noise. Third, results from adjacent postures were cross-checked to recover "missing peaks" caused by sensor placement issues (e.g., nodal points). Finally, stabilization diagrams validated the consistency of identified peaks. By testing the robot in closely spaced postures and systematically verifying results across neighboring postures, this approach minimized errors and ensured reliable modal parameters for analyzing vibrational behavior. This method effectively addressed challenges in the dynamic testing of posture-dependent robots.

B. Observational Analysis of Robot Vibration Behavior

In this section, the collected and analyzed data derived from hammer tests are used to study the vibration behavior of the robot manipulators. The heatmap in Figure 2 shows the correlation between the joint angles (J1, J2, J3) and the first three low-frequency vibration modes (Mode 1, Mode 2, Mode 3) of a robot manipulator.

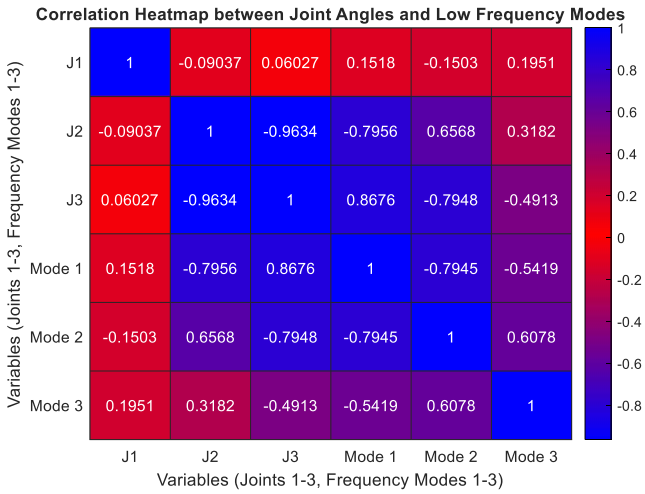

Figure 2: Correlation heatmap between joint angles (1, 2, and 3) and low-frequency modes (1, 2, and 3).

By considering the correlation diagram in Figure 2, we can provide a more detailed analysis of the vibrational behavior in low-frequency modes. This diagram indicates that the significance of changes in the angles of joints 2 and 3 is substantially greater than that of joint 1, as they exhibit larger coefficients. This indicates that the most energy absorption by low-frequency modes is caused by the movement of joints 2 and 3 of the robot. However, components that interact with external forces (e.g., the end-effector) can introduce additional vibrations. The energy absorbed or transmitted by each component affects its contribution to specific vibration modes [14]. In fact, it can be said that the energy absorbed or transmitted by each component influences its contribution to specific vibration modes through modal participation factors and mode shapes. In general, flexible arms in industrial robots may experience internal resonance between bending and torsional modes which affects precision [15]. To handle this complicated problem, using a model that can accurately predict the system's vibration patterns is a challenge.

III. Mathematical Analysis of Higher Vibration Modes

The dynamics of the robotic manipulator (as shown in Figure 1) can be described by the equations of motion as follows:

$$\boldsymbol{M}\ddot{\mathbf{x}}(t) + \boldsymbol{C}\dot{\mathbf{x}}(t) + \boldsymbol{K}\mathbf{x}(t) = \boldsymbol{f}(t) \tag{1}$$

where, $\boldsymbol{M}$ is the mass matrix which depends on the distribution of masses across links and joints, $\boldsymbol{C}$ is the damping matrix which describes energy dissipation in the system, $\boldsymbol{K}$ is the stiffness matrix which accounts for elastic properties of links and joints, $\mathbf{x}$ is the generalized coordinate vector and $\boldsymbol{f}$ is the external force vector. The eigenvalue problem for free vibration is obtained by assuming a harmonic solution of $(x(t) = \phi e^{i\omega t})$ and no external forces $(\boldsymbol{f} = 0)$ and neglecting damping $(\boldsymbol{C} = 0)$:

$$\boldsymbol{K\Phi} = \boldsymbol{M\Phi\Lambda}, \tag{2}$$

where, $\boldsymbol{\Phi}$ is the matrix of mode shapes (eigenvectors), and $\boldsymbol{\Lambda}$ is the diagonal matrix of eigenvalues. Each mode shape ϕ_i

Identify applicable sponsor/s here. *(sponsors)*

represents a deformation pattern of the system at the corresponding natural frequency ω_i.

Now, the response of the system under external excitation is governed by the modal superposition principle:

$$\mathbf{x}(t) = \sum_{i=1}^{N} \phi_i \eta_i(t) \tag{3}$$

where, ϕ_i is the i-th mode shape, $\eta_i(t)$ is the time-dependent modal coordinate. The contribution of each mode depends on the modal participation factor:

$$\Gamma_i = \phi_i^{\top} \boldsymbol{f} \tag{4}$$

higher modes often have smaller participation factors because they involve localized dynamics (smaller deformations with less energy) [16]. Lower modes dominate as they involve global deformations that absorb more energy. On the other hand, for higher modes, the mode shapes ϕ_i involve vibration in smaller substructures or localized parts such as the end-effector. In addition, these localized vibrations have higher natural frequencies and smaller deformation amplitudes which make them less sensitive to global changes in posture. Now, by mathematically defining FRF, we have:

$$\mathbf{H}(\omega) = (\boldsymbol{K} - \omega^2 \boldsymbol{M} + j\omega \boldsymbol{C})^{-1} \tag{5}$$

and breaking this into modal contributions:

$$\mathbf{H}(\omega) = \sum_{i=1}^{N} \frac{\phi_i \phi_i^{\top}}{\lambda_i - \omega^2 + j\omega\zeta_i\omega_i}, \tag{6}$$

where, $\zeta_i = \frac{c_i}{2\sqrt{k_i m_i}}$ is the damping ratio for the mode i.

The two main results of this section are as follows:

1. Lower modes absorb more energy due to their higher participation in external excitation, whereas higher modes dissipate energy locally and less effectively contribute to the overall response,
2. Lower modes correspond to global deformation patterns, while higher modes involve localized dynamics.

These outcomes are observed when joints 2, and 3 significantly alter the robot's posture.

At the end of this section, the vibration analysis showed that the wrist joints (joints 4, 5, and 6) do have some impact on the lower frequency modes, but joints 2 and 3 have a stronger influence on the main vibration modes. To make the GPR model more accurate, we included all six joints of the robot as inputs for training the model. This ensures that the model takes into account the contributions of all joints, even those with less impact, to predict important modal parameters like frequencies, damping ratios, and stiffnesses. Using the experimental data, the GPR model provides reliable predictions of the robot's FRFs, forming a strong basis for further analysis.

A. Gaussian Process Regression (GPR) model

In this section, to predict the modal parameters of the robot manipulators, including natural frequency, damping ratio, and modal stiffness in three directions (X, Y, and Z) in a given posture, the GPR method, which is an interpolation method based on the correlation between different input data points, was employed [17]. The schematic of the GPR model is shown in Figure 3. As shown in Figure 3, the preprocessing stage of the dataset in the GPR algorithm involves augmenting the dataset to ensure it reaches an appropriate accuracy level during training and to prevent underfitting and overfitting of the data. In addition, the dataset is divided into two categories consisting of 90% training dataset and 10% testing dataset. The last 15 postures were used for comparison with predicted data.

The modal parameters of the robot for a given posture using the Gaussian process are defined as follows [12, 18, 19]:

$$g(\mathrm{x}) \sim \boldsymbol{GP}\big(\mu(\mathrm{x}), \mathbf{C}(\mathrm{x}, \mathrm{x}^*)\big), \tag{7}$$

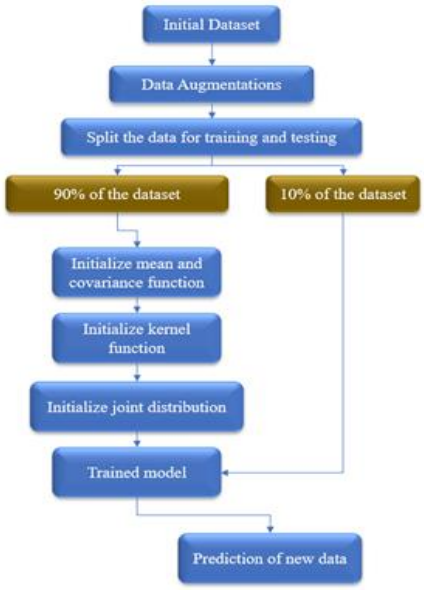

Figure 3: The schematic of the Gaussian Process Regression (GPR) model.

where, in equation (7), $\mu(\mathrm{x})$ is the basic function, and x represents the joint positions for all training robot postures. $\mathbf{C}(\mathrm{x}, \mathrm{x}^*)$ is the covariance matrix for the training data. The covariance matrix, $\boldsymbol{k}(\mathrm{x_i}, \mathrm{x_j})$, for the postures is calculated using a squared exponential kernel function:

$$\boldsymbol{k}(x_i, x_j) = \sigma_f^2 exp\left(-\frac{(x_i - x_j)^T (x_i - x_j)}{2\sigma_l}\right), i \neq j \tag{8}$$

where σ_l is the feature length and σ_f is the standard deviation of the signal. x_i and x_j are the vectors of joint positions at the corresponding postures. Now, for a series of predicted positions, the prior results are:

$$\begin{bmatrix} g(x) \\ g(x_*) \end{bmatrix} \sim N\left(\begin{bmatrix} \mu(x) \\ \mu(x_*) \end{bmatrix}, \begin{bmatrix} \mathbf{C}(x,x) + \sigma^2\mathbf{I} & \mathbf{C}(x,x_*) \\ \mathbf{C}(x_*,x) & \mathbf{C}(x_*,x_*) \end{bmatrix}\right), \quad (9)$$

here, in equation (9), σ^2 is the model variance, and I is the identity matrix. x represents the joint positions of all training robot postures, and x_* represents the joint positions of the test postures. $\mathbf{C}(x,x)$, $\mathbf{C}(x,x_*)$, and $\mathbf{C}(x_*,x_*)$ are the covariance moments of the training samples, the covariance matrix between the training and test samples, and the covariance matrix of the test samples, respectively. These are used to predict the posterior distribution through Bayesian inference, and its mean can be expressed as:

$$g(x_*) = \mu(x_*) + \mathbf{C}(x_*,x)[\mathbf{C}_{tr}(x,x) + \sigma^2\mathbf{I}]^{-1}(f_{tr}(x) - \mu_{tr}) \quad (10)$$

In this case, $f_{\mathrm{tr}}(x)$ represents the predicted parameter values, and μ_{tr} is their average. Before training the model using equation (8), it is necessary to determine the best hyperparameters (σ_l, σ_f^2) through a process called maximum likelihood estimation [18]:

$$L = -\frac{1}{2}f_{\mathrm{tr}}^{\mathrm{T}}(\boldsymbol{x})\mathbf{C}_n^{-1}f_{\mathrm{tr}}(\boldsymbol{x}) - \frac{1}{2}\log|\mathbf{C}_n| - \frac{\boldsymbol{M}}{2}\log(2\pi), \quad (11)$$

in which, $\mathbf{C_n} = \mathbf{C_{tr}}(x,x) + \boldsymbol{\sigma^2}\mathbf{I}$ is the covariance matrix of the training data in the noise condition.

IV. Results and Discussion

In this section, the results of the predicted modal parameters, including natural frequencies, damping ratios, and modal stiffness obtained using the GPR model, are first presented. In the second part, graphs of FRFs generated with these modal parameters are compared with measured FRFs. This comparison demonstrates the high accuracy of the GPR model.

A. *Presentation of GPR Results*

The GPR model used in this research is a non-parametric, probabilistic tool for predicting modal parameters, including natural frequencies, damping ratios, and modal stiffness, of the robot manipulator across various postures. By using a dataset derived from the EMA after a comprehensive vibrational analysis, the GPR model uses joint angles as inputs and computes the posterior distribution of modal parameters by learning their covariance structure. A squared exponential kernel function is employed to model the relationships between joint angles and modal parameters. It ensures smoothness and flexibility in predictions. Hyperparameters of the kernel are optimized using maximum likelihood estimation to improve accuracy. The GPR model efficiently captured the posture-dependent behavior of the robot and provided reliable predictions with a Mean Squared Error (MSE) of 0.00387. The computations were performed on a PC with 32 GB of RAM and an x64-based i7 CPU.

In Figure 4, the results obtained from the GPR model for the natural frequencies, damping ratios and modal stiffnesses in the first four vibration modes are compared with experimental results. This comparison has been performed for the last fifteen end-point postures along the designed trajectory.

In plots of damping ratios, they have a wide area of confidence interval which indicates higher uncertainty in the model's prediction. The complexity and minor errors in calculating the damping ratio are attributed to control parameters, friction, and sensitivity to nonlinear variations [20].

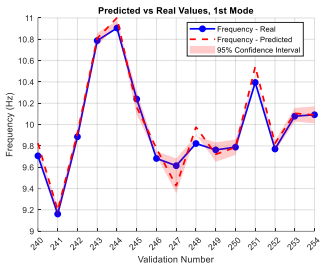

Frequency-Mode 1

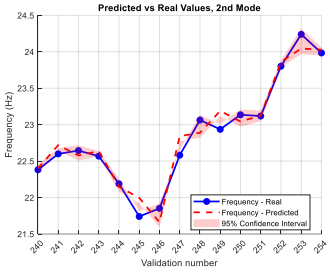

Frequency-Mode 2

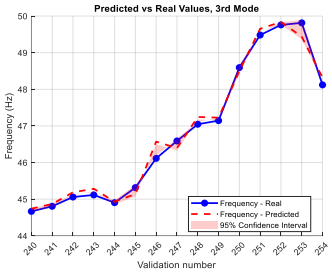

Frequency-Mode 3

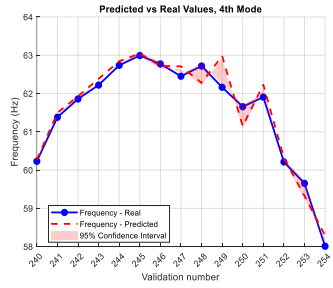

Frequency-Mode 4

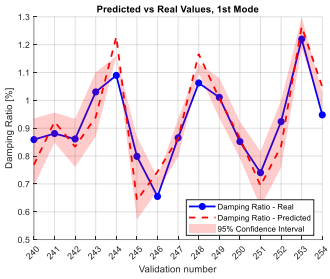

Damping ratio-Mode 1

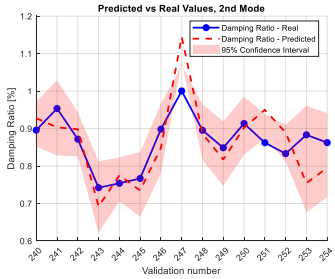

Damping ratio-Mode 2

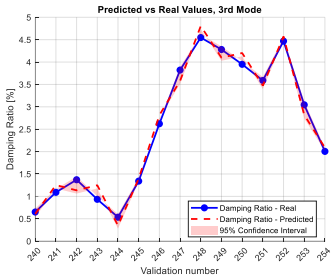

Damping ratio-Mode 3

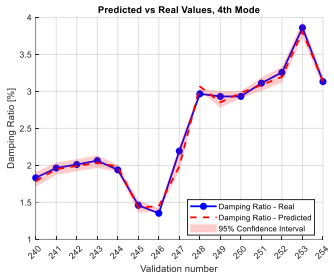

Damping ratio-Mode 4

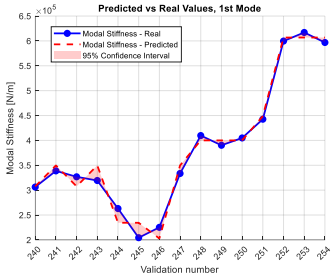

Modal stiffness-Mode 1

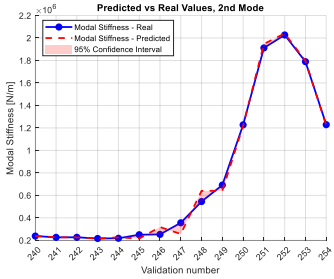

Modal stiffness-Mode 2

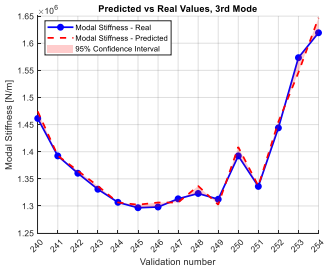

Modal stiffness-Mode 3

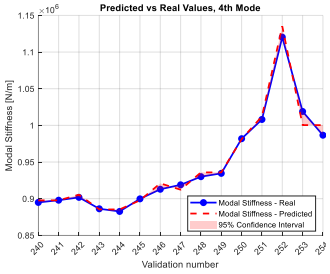

Modal stiffness-Mode 4

Figure 4: The prediction of the natural frequency, damping ratio and modal stiffness extracted from the GPR model for the first 4 vibration modes.

B. *Estimation of Frequency Response Function (FRF)*

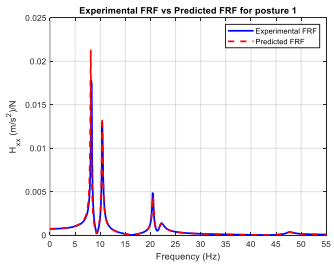

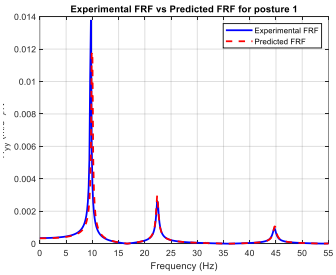

Posture 250-Direction X Posture 250-Direction Y

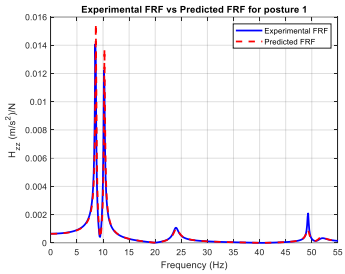

Posture 250-Direction Z

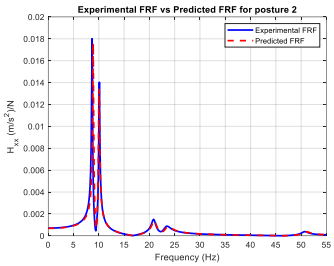

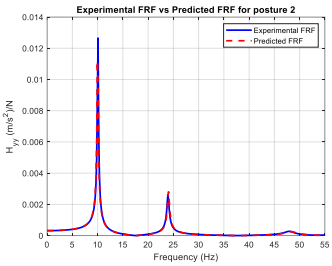

Posture 251-Direction X Posture 251-Direction Y

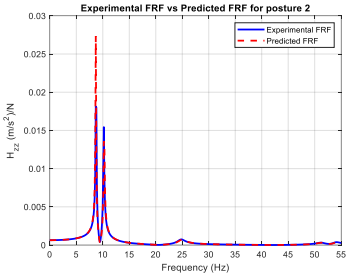

Posture 251-Direction Z

Figure 5: The prediction of the natural frequency, damping ratio and modal stiffness extracted from the GPR model for the first 2 vibration modes.

As investigated in section 2, the focus on low frequencies is due to the direct correlation of the first few frequencies with the primary vibration modes. These modes exhibit significant deformations and account for a substantial portion of the vibrational energy along the excitation direction. Therefore, we aim to estimate the diagonal FRFs aligned with the external excitation direction. Consequently, in the FRF matrix, our goal is to construct the diagonal FRFs H_{xx}, H_{yy} and H_{zz}.

V. CONCLUSIONS

This research studied the vibration behavior of robot manipulators using a structured experimental and analytical approach. A tool-tip trajectory was designed, and hammer tests were conducted in the X, Y, and Z directions to measure diagonal FRFs and avoid cross-effects. Two major challenges were addressed: understanding how the robot's posture affects

vibration modes and how the accelerometer's placement on nodal or anti-nodal points influences the results. To accurately identify vibration peaks, hammer tests were carried out on 254 robot postures using a four-stage peak-selection process, which helped identify key vibration modes. A dataset was then created, including joint angles and modal parameters such as natural frequencies, damping ratios, and stiffnesses. This dataset was used to train a GPR model, which effectively predicted posture-dependent vibration behavior. The results of the prediction show that the GPR model can manage the complex vibration patterns in the robot manipulators. The GPR model also reduced computational costs while maintaining high accuracy. Finally, the predicted modal parameters were used to construct FRFs for machining postures, and these were validated against experimental results. This study provides a clear method for analyzing robot vibrations, improves the understanding of how joint angles influence vibrations, and offers a practical approach for efficient vibration analysis in industrial applications, particularly robotic machining.

ACKNOWLEDGMENT

This work has been supported by the National Research Council Canada (NRC). The authors thank the NRC technical team, particularly the Robotics and Hybrid Manufacturing teams at the Aerospace Manufacturing Technologies Centre. Furthermore, the financial support of the Natural Sciences and Engineering Research Council of Canada (NSERC) through the Discovery Grant is also acknowledged.

REFERENCES

[1] A. Verl, A. Valente, S. Melkote, C. Brecher, E. Ozturk, and L. T. Tunc, "Robots in machining," *CIRP Annals*, vol. 68, no. 2, pp. 799–822, 2019.

[2] W. Ji and L. Wang, "Industrial robotic machining: A review," *The International Journal of Advanced Manufacturing Technology*, vol. 103, pp. 1239–1255, 2019.

[3] L. Yuan, Z. Pan, D. Ding, S. Sun, and W. Li, "A review on chatter in robotic machining process regarding both regenerative and mode coupling mechanism," *IEEE/ASME Transactions on Mechatronics*, vol. 23, no. 5, pp. 2240–2251, 2018.

[4] Y. Altintaş and E. Budak, "Analytical prediction of stability lobes in milling," *CIRP Annals*, vol. 44, no. 1, pp. 357–362, 1995.

[5] J. Munoa, X. Beudaert, Z. Dombovari, Y. Altintas, E. Budak, C. Brecher, and G. Stepan, "Chatter suppression techniques in metal cutting," *CIRP Annals*, vol. 65, no. 2, pp. 785–808, 2016.

[6] A. Maamar, V. Gagnol, T. P. Le, and L. Sabourin, "Pose-dependent modal behavior of a milling robot in service," *The International Journal of Advanced Manufacturing Technology*, vol. 107, pp. 527–533, 2020.

[7] Y. Mohammadi and K. Ahmadi, "In-process frequency response function measurement for robotic milling," *Experimental Techniques*, vol. 47, no. 4, pp. 797–816, 2023.

[8] Y. Peng, B. Li, X. Mao, H. Liu, C. Qin, and H. He, "A method to obtain the in-process FRF of a machine tool based on operational modal analysis and experiment modal analysis," *The International Journal of Advanced Manufacturing Technology*, vol. 95, pp. 3599–3607, 2018.

[9] I. Iglesias, M. A. Sebastián, and J. E. Ares, "Overview of the state of robotic machining: Current situation and future potential," *Procedia Engineering*, vol. 132, pp. 911–917, 2015.

[10] V. Nguyen, T. Cvitanic, and S. Melkote, "Data-driven modeling of the modal properties of a six-degrees-of-freedom industrial robot and its application to robotic milling," *Journal of Manufacturing Science and Engineering*, vol. 141, no. 12, 121006, 2019.

[11] V. Nguyen and S. Melkote, "Hybrid statistical modelling of the frequency response function of industrial robots," *Robotics and Computer-Integrated Manufacturing*, vol. 70, 102134, 2021.

[12] K. Deng, D. Gao, C. Zhao, and Y. Lu, "Prediction of in-process frequency response function and chatter stability considering pose and feedrate in robotic milling," *Robotics and Computer-Integrated Manufacturing*, vol. 82, 102548, 2023.

[13] N. T. Alberto, M. Mistry, and F. Stulp, "Computed torque control with variable gains through Gaussian process regression," in *2014 IEEE-RAS International Conference on Humanoid Robots*, 2014, pp. 212–217.

[14] H. Song, X. Shan, H. Yu, G. Wang, and J. Fan, "Influences of parameter deviation on the vibration isolation system of an end effector," *Actuators*, vol. 11, no. 5, p. 133, May 2022.

[15] A. I. Manevich, & L. I. Manevich, "The mechanics of nonlinear systems with internal resonances." *World Scientific*, 2005.

[16] W. A. Hashlamoun, M. A. Hassouneh, and E. H. Abed, "New results on modal participation factors: Revealing a previously unknown dichotomy," *IEEE Transactions on Automatic Control*, vol. 54, no. 7, pp. 1439–1449, 2009.

[17] M. Ebden, "Gaussian processes for regression: A quick introduction," *The Website of Robotics Research Group in Department of Engineering Science, University of Oxford*, vol. 91, pp. 424–436, 2008.

[18] H. Chen and K. Ahmadi, "Estimating pose-dependent FRF in machining robots using multibody dynamics and Gaussian Process Regression," *Robotics and Computer-Integrated Manufacturing*, vol. 77, 102354, 2022.

[19] V. Nguyen, J. Johnson, and S. Melkote, "Active vibration suppression in robotic milling using optimal control," *International Journal of Machine Tools and Manufacture*, vol. 152, 103541, 2020.

[20] L. T. Tunc and B. Gonul, "Effect of quasi-static motion on the dynamics and stability of robotic milling," *CIRP Annals*, vol. 70, no. 1, pp. 305–308, 2021.